Exploring lignin valorisation: the application of photocatalysis for the degradation of the β-5 linkage

Murnaghan, C. W. J., Skillen, N., Hardacre, C., Bruce, J., Sheldrake, G. N., & Robertson, P. K. J. (2021). Exploring lignin valorisation: the application of photocatalysis for the degradation of the β-5 linkage. *Journal of Physics: Energy*, *3*(3), Article 035002. https://doi.org/10.1088/2515-7655/abf853

Published in:
Journal of Physics: Energy

Document Version:
Publisher's PDF, also known as Version of record

JPhys Energy

PAPER • OPEN ACCESS

Exploring lignin valorisation: the application of photocatalysis for the degradation of the β-5 linkage

IOP Publishing J. Phys. Energy 3 (2021) 035002 https://doi.org/10.1088/2515-7655/abf853

Journal of Physics: Energy

OPEN ACCESS

RECEIVED
25 November 2020

REVISED
13 April 2021

ACCEPTED FOR PUBLICATION
15 April 2021

PUBLISHED
19 May 2021

PAPER

Exploring lignin valorisation: the application of photocatalysis for the degradation of the β-5 linkage

Christopher W J Murnaghan[1,3], Nathan Skillen[1,2,3], Christopher Hardacre[2], John Bruce[1], Gary N Sheldrake[1] and Peter K J Robertson[1,*]

[1] School of Chemistry and Chemical Engineering, David Keir Building, Stranmillis Road, Queens University Belfast, Belfast BT9 5AL, Northern Ireland, United Kingdom
[2] Department of Chemical Engineering and Analytical Science, The Mill, Sackville Street, University of Manchester, Manchester M1 3AL, United Kingdom
[3] Authors contributed equally to this work
[*] Author to whom any correspondence should be addressed.

E-mail: g.sheldrake@qub.ac.uk **and** p.robertson@qub.ac.uk

Keywords: lignin valorisation, photocatalysis, titanium dioxide, β5 linkage, UV LED

Supplementary material for this article is available online

Abstract

The valorisation of lignin has gained significant interest in bioenergy, which is driven by the abundance of the material coupled with the potential to form value-added compounds. As a result, the range of technologies deployed for this application has increased and more recently includes advanced oxidation processes such as photocatalysis. The complexity of lignin is challenging however, and therefore model compounds, which represent key linkages in the native structure, have become crucial as both a tool for evaluating novel technologies and for providing an insight into the mechanism of conversion. Previously, the β-O-4 dimer, the most abundant linkage found in native lignin, has been extensively used as a model compound. Described herein, however, is the first report of photocatalytic TiO_2 technology for the degradation of a β-5 model dimer. Under low power UV-light emitting diode irradiation, complete degradation of the β-5 compound (6.3×10^{-3} mg ml^{-1} min^{-1}) was achieved along with formation and subsequent removal of reaction intermediates. Investigation into the mechanism revealed within the first 2 min of irradiation there was the formation of a diol species due to consumption of the alkene sidechain. Although the data presented highlights the complexity of the system, which is underpinned by multiple oxidative reaction pathways, an overview of the key photocatalytic processes are discussed including the impact of acetonitrile and role of reactive oxygen species.

1. Introduction

The use of photocatalysis for biomass valorisation has grown significantly with an increasing number of papers now being reported in the literature [1–9]. To date, cellulose has typically been used as a model compound for biomass and has been proven to be a potentially sustainable feedstock and sacrificial electron donor for photocatalytic H_2 production [2–7]. As a result, focus has now started to shift towards raw biomass conversion and subsequently the challenge of photocatalytic biomass reforming and specifically lignin depolymerisation [5, 8–10].

While the conversion of lignin is challenging, there is significant potential to generate a range of value-added products. Despite examples in the literature demonstrating that raw biomass conversion can be achieved via photocatalysis [9], very few have investigated the more fundamental challenges associated with the chemistry of lignin photoreforming. This is a crucial consideration regarding advancing photocatalytic technology as recently stated by Wang *et al*, facilitating the knowledge transfer is reliant on not just improving reactor design and optimisation but also addressing the fundamental chemistry challenges [11].

Previously, studies have shown that the degradation of lignin-containing chemical pulps and two soluble lignins was achievable using photocatalytically generated reactive oxygen species (ROS) such as OH radicals ($OH^{\bullet}$), superoxide radical anions ($O_2^{\bullet -}$) and singlet oxygen [12–14]. Lignin, however, is composed of a series of key bonding patterns formed from the radical combination of monolignols [15], with the β-O-4, β-5 and 5–5′ biphenyl linkages being the most abundant. Considering the lignin content of softwood species, the varying relative proportions of β-O-4, β-5 and 5–5′ biphenyl are 45%–50%, 9%–12% and 19%–22%, respectively [16]. A number of reports in the literature have focused on synthesising model compounds which contain these linkages and vary in complexity [17–20]. The degradation of these compounds has traditionally been achieved using oxidative and reductive catalysis [21–25], along with ionic liquid-mediated breakdown [26, 27]. While limited, the majority of previously reported photocatalysis research in this field has concentrated on the degradation of only β-O-4 lignin models [12, 28–33]. To date, the degradation of β-5 models has rarely been explored [34, 35] and furthermore, has never been reported using photocatalysis.

As stated above, previous research has focused on photocatalysis of the β-O-4 linkage in an attempt to yield valuable products with high selectivity under visible light irradiation [36]. Interestingly, very few of these studies have utilised TiO_2, which remains the most commercially available and active photocatalyst material. This limited use may be a result of the apparent limitations associated with the material. While UV light is required for TiO_2 photo-excitation, it is worth noting the majority of visible light studies still typically use artificial light sources, which often have significant power requirements. With advances in light emitting diode (LED) technology, the coupling of TiO_2 and UV-LEDs presents an approach where an energy efficient system could be created that minimises the limitations of TiO_2 not being activated by visible light. In addition, the wider band potential of TiO_2 also means the material has a strong oxidising potential at the valence band (typically 2.8–2.9 eV vs NHE) and can produce powerful radicals (e.g. $OH^{\bullet}$), which could be of importance when the complexity of larger models or lignin itself is considered. This may be crucial, as it is vital that any approach utilised for lignin valorisation is capable of degrading a range of key linkages present in this complex material.

Therefore, reported herein, is the first application of UV–TiO_2 photocatalysis for the degradation of β-5 along with the identification of reaction intermediates. The data presented are the initial findings in an ongoing investigation that is focused on providing a crucial insight into the mechanism of lignin conversion with a view towards establishing an improved method of valorisation.

2. Methods

2.1. (*E*)-2-methoxy-4-(7-methoxy-3-methyl-5-(prop-1-en-1-yl)-2,3-dihydrobenzofuran-2-yl)phenol (β-5)

Isoeugenol (5.0 g, 30 mmol) was dissolved in water and EtOH (25 ml and 57 ml, respectively). To this was added $FeCl_3$ (2.96 g, 18.2 mmol, 0.6 eq). The flask was stoppered and shaken vigorously for 30 s and then stored in the freezer for 3 d. The mixture was filtered under vacuum and the solid washed with ice-cold EtOH. The crystalline product was then resuspended in a minimum quantity of DCM and passed through a short silica plug, where then the plug was washed with DCM (100 ml) and the filtrate concentrated to provide the product as a white solid (0.94 g, 19% yield). ^{1}H NMR (400 MHz, $CDCl_3$) δ_H ppm 1.38 (3 H, d, $J = 6.77$ Hz, γ'-H), 1.87 (3 H, d, $J = 6.53$ Hz, γ''-H), 3.45(1H, m, β'-H), 3.88(3 H, s, OMe), 3.89(3 H, s, OMe), 5.10(1H, d, $J = 9.45$ Hz, α'-H), 5.62(1H, s, OH), 6.12(1H, m, $J = 15.68$ Hz, 6.59 Hz, Ar), 6.90(2 H, s, Ar), 6.97(1 H, s, Ar). ^{13}C NMR (400 MHz, $CDCl_3$) δ_H ppm 17.57, 18.40, 45.64, 55.94, 55.99, 93.92, 108.93, 109.23, 113.32, 114.08, 120.00, 123.52, 130.94, 132.1, 132.22, 133.28, 144.17, 145.79, 146.59, and 146.68. Values consistent with reported literature [18].

2.2. Photocatalytic experiments

Photocatalytic experiments were carried out in a simple experimental set up that consisted of a stirred beaker with irradiation provided by a single overhead UV-LED positioned approximately 100 mm from the top of the reaction solution. In a typical experiment, a predetermined weight of lignin model substrate was dissolved in a 100 ml solution of 50:50 water and CH_3CN. In addition, a loading of 0.5 g l^{-1} TiO_2 P25/P20 (Evonik) was also added to the reaction solution. The reaction solution was continuously stirred throughout the experiment using a magnetic stirrer bar and plate. Each reaction was kept in the dark for 30 min prior to irradiation to allow for equilibrium. Irradiation was provided by a UV-LED (Series ILH-Xx01-Sxxx-SC211-WIR200, Intelligent LED Solutions) with a peak wavelength at 375 nm and 65° viewing angle, operated at a $V_F = 14$ dcV and $I_F = 0.25$ A, which was powered by a dedicated bench top DC power supply (TENMA). The LED was mounted onto a 50 (outer diameter) × 80 (length) mm heatsink (Intelligent LED solutions). The irradiance of the LED was measured using a radiometer (UV–X) at a distance of 70 and 120 mm from the source, which represented the top and base of the 100 ml reaction medium. The LED

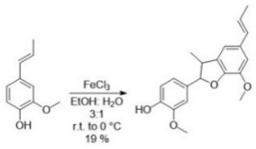

Scheme 1. Synthesis of the β-5 linkage by dimerisation of isoeugenol using iron (III) chloride [40].

intensity was measured to be 19.5 and 6.8 mW cm^{-2} at 70 and 120 mm, respectively. In addition, figure S2 (available online at stacks.iop.org/JPENERGY/3/035002/mmedia) provides a spectral output of the lamp as measured by a StellarNet BLACK-comet concave grating spectrometer, which confirms a peak wavelength of 375 nm (StellarNet Inc.). Samples (1.5 ml) were taken periodically during irradiation and centrifuged at 15 000 rpm for 15 min to separate the supernatant from the catalyst prior to analysis. All experiments were conducted in duplicate ($n = 2$) and control experiments were performed in the absence of light (dark control) and catalyst (photolysis/light control).

Analysis of reaction samples was performed by UV–visible spectroscopy, HPLC–UV, LC–MS and NMR spectroscopy. UV–visible spectroscopy was carried out using a Cary 300 Scan UV–visible spectrometer (see figures S3 and S4 for standards). A quartz cell was used to analyse 1 ml aliquots from the reaction solution with a scan range of 800–190 nm at a rate of 400 nm min^{-1}.

For HPLC–UV analysis, an Agilent 1100 HPLC system equipped with a photodiode array UV–Vis was used. A Phenomenex Kinetex^{R} C18 analytical column (150 mm $\times$ 4.6 mm, 100 Å) was used, and the mobile phase was (A) 0.2% acetic acid and (B) methanol over the following gradient: 50:50 (A:B) to 100% B (0–6 min) and then back to 50:50 (A:B) (6–10 min). The flow rate was 1 ml min^{-1} and the injection volume was 5 μl. Under these conditions β-5 eluted at 5.901 min and was identified based on comparison to a standard (see figures S5 and S6).

NMR spectroscopic experiments were conducted in a 100 mm long quartz tube with a 12 mm diameter. Agitation was provided by magnetic stirring at the base of the tube and irradiation was delivered from the side using the same LED as previously shown in figure S2. The reaction solution composition was as follows: β-5 dimer (50 mg) was dissolved into 3 ml total solution by the addition of CD_3CN (2.25 ml) and H_2O (0.75 ml). An initial sample (T_0) was removed from the quartz tube and analysed on a Bruker Avance 400 MHz spectrometer and the residual solvent peak of CD_3CN was set to $\delta = 1.94$. Following this, the aliquot removed for NMR analysis was then returned to the quartz tube and TiO_2 (50 mg) was added. The tube was irradiated over a 36 h period and sampled at time points 0, 6, 12, 24 and 36 h. For the sampling of the reaction, the irradiation was stopped, and 0.6 ml of the reaction mixture was removed, centrifuged in an Eppendorf tube and the supernatant analysed by NMR spectroscopy. The solution was then added back to the Eppendorf to resuspend the catalyst and transferred back to the quartz tube before irradiation was resumed.

LC–MS analysis was performed on an Agilent 1260 Infinity II with an InfinityLab LC/MSD equipped with a Kinetex 5 μm C18, LC column 150 $\times$ 4.6 mm. Chromatography was carried out using two solvents: (A) water and 0.1% formic acid solution and (B) acetonitrile and 0.1% formic acid solution. The gradient followed is 0–6 min 50% solvent A 50% solvent B and 6–12 min 100% solvent B. The flow rate was 1.0 ml min^{-1} with an injection volume of 5 μl, and the column temperature was 25 °C. The detector on the LC was a VWD measuring the wavelength at 275 nm. The mass detector was in negative mode and the machine is ESI–MS. A chromatogram and mass spectrum of a β-5 standard is shown in ESI (figure S7).

3. Results and discussion

3.1. Photocatalytic degradation of β-5

While lignin models, and specifically those with β-O-4 linkages, have been extensively reported in the literature, there are only a limited number of examples that have used TiO_2 photocatalysis as a method of degradation [37]. Moreover, there are currently no examples of photocatalysis being used for the degradation of the β-5 linkage. The method used for the synthesis of the model is also rarely reported in the literature (scheme 1), as typically the enzyme Horse Radish Peroxidase [38] or an acid-catalysed ring closure [30] are employed. In contrast, oxidative coupling using iron (III) chloride provided the β-5 dimer for this study, which is a method that has not been used extensively since 1950 [39].

The data presented in figure 1 demonstrates the degradation achieved using TiO_2 photocatalysis for the lignin β-5 linkage model. Complete removal of the β-5 model (to the limit of detection) was achieved within 45 min of UV-LED irradiation with a degradation rate of 6.3 $\times$ 10^{-3} mg ml^{-1} min^{-1} achieved during the first 30 min of irradiation. In addition, a plot of ln[β-5] vs time (figure 1(b)) confirmed the reaction to be

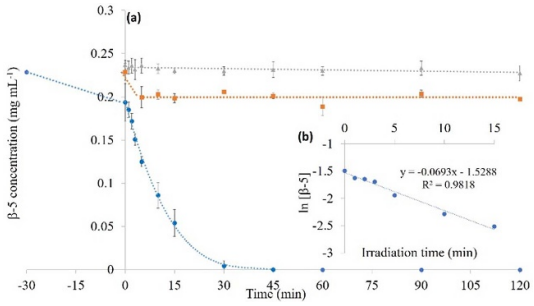

Figure 1. Photocatalytic degradation of β-5 where (a) is the time-concentration profile under photocatalytic (●), photolytic (▲) and catalyst only conditions (■) (0 min represents when illumination was started for photocatalytic and photolytic conditions) and (b) is a plot of ln[β-5] vs time.

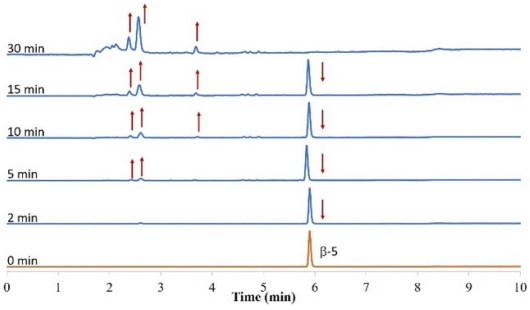

Figure 2. Stacked HPLC chromatograms detailing the photocatalytic degradation of β-5 and formation of reaction intermediates across a 30 min irradiation period. For clarity, the red arrows indicate the increase and decrease of peak areas.

first order during this period. The figure also shows the process was driven by photocatalysis with no significant degradation observed under photolytic conditions. Adsorption of the β-5 model to the surface of TiO_2 (15.24%) was noted during dark control experiments and as such the reaction was given 30 min prior to irradiation (denoted as −30 to 0 min in figure 1(a)) to reach equilibrium. The adsorption of the compound to the surface also confirmed that complete CH_3CN saturation had not occurred and that the interaction between TiO_2 and adsorbed β-5 was likely facilitating degradation.

Alongside the degradation of β-5, the formation of reaction intermediates was also monitored, (figure 2). Prominent peaks were detected at retention times (R_t) of 2.38, 2.57 and 3.71 min and formed after 2 min ($R_t = 2.38$ and 2.57 min) and 5 min ($R_t = 3.71$ min) irradiation. The peak areas for all compounds were observed to increase up to 30 min of irradiation, whereafter a decrease was noted with minimal detection after 120 min irradiation (figure S8). The decrease observed was likely a result of subsequent oxidation, which was accelerated by the near complete removal of the peak at $R_t = 5.87$ min (which corresponded to β-5) after 30 min. These observations suggest that photocatalysis was capable of achieving complete degradation of the lignin linkage, including the formation and subsequent removal of reaction intermediates.

3.2. Reaction intermediates and mechanism

While complete removal (to the limit of detection) of β-5 was achieved (figure 1), this was coupled with evidence for the formation of several reaction intermediates (figure 2). Determining the full mechanistic pathway for such a compound is challenging; however, the work conducted herein, has identified the initial compounds forming in the reaction solution, which are detailed in figure 3.

LC–MS analysis (ESI figures S10–S13 for mass spectra) confirmed **P1** was the initial compound formed in the reaction pathway (detected after 2 min of irradiation) resulting from hydroxyl radical-driven consumption of the side-chain alkene. This reaction has previously been reported in other photocatalytic applications as the initial process occurring during oxidative degradation in a TiO_2 system [41, 42]. Work by Liu *et al* showed during the photocatalytic degradation of cyanotoxin microcystin-LR, one of the first reactions was ROS attack at the unsaturated side chain to produce a diol species, similar to that found in **P1**. This observation was also the subject of work by Feltham *et al* and Goulay *et al* who postulated the transition state for the formation of a diol species arising from the abstraction of a proton β to the alkene under attack from the OH radical [43, 44].

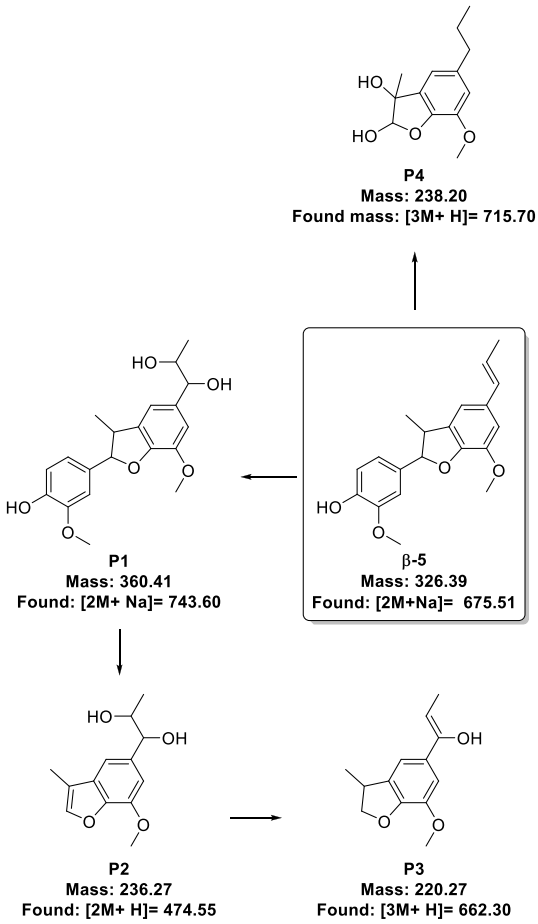

Figure 3. Proposed products identified from LC–MS analysis. Products labelled P1-4 are not a cascade degradation pathway and are speculatively proposed to be forming from multiple oxidation reactions (mass spectra can be seen in ESI figures S10–S13).

The formation of **P2** was proposed to be as a result of the elimination of the guaiacyl side chain which provided the alkene within the furan ring. The conditions under which this elimination occurred would be the abstraction of either protons labelled in figure 4 as Hα' or Hβ'. In relation to the other proposed product in figure 3, the formation of **P3** which occurs again at the propyl sidechain, appears to have arisen in **P3** from the abstraction of the H–α'' resulting in an elimination reaction and the formation of the alkene species. The formation of product **P4** is plausible as it follows a similar pathway to the substrate whereby the formation of an alkene within the furan ring is consumed by the hydroxyl radicals within the bulk to provide the diol, which was also observed in the formation of **P1**.

To further support these observations, NMR spectroscopic analysis was performed which traced the progress of the β-5 model degradation over a prolonged irradiation time frame, figures 5 and 6. From figure 5 it can be seen that at 5.06 ppm, the doublet which corresponds to Hα' is undergoing a change of environment hence the removal of the doublet along the reaction course. Almost complete disappearance of the doublet after 36 h of irradiation was also observed showing that this structural feature was being completely removed. This observation in the NMR spectra is in good agreement with the LC–MS data where the elimination of the guaiacyl side chain from the model substrate was seen. The changes observed in the NMR spectra correspond to cleavage of the carbon–carbon bond between the guaiacol and the furan unit. The formation of a triplet at 4.85 ppm also suggests the formation of an intermediate species which bears a newly formed CH_2 group. This intermediate, however, was assumed to undergo further degradation, which was evident from the decrease in the integral of the triplet after 36 h owing to its assumed lack of stability.

The doublet at 1.26 ppm corresponds to the $CH_3\gamma'$ on the model dimer and following 24 h of irradiation, was completely removed. This observation points towards the chemical environment of the exocyclic methyl group changing, which could be explained by the formation of products **P2** or **P4** (figure 6.). Also seen in figure 5 is the doublet of doublets at 1.76 ppm which corresponds to the $CH_3\gamma''$ on the alkene in the substrate which also disappeared during the 36 h irradiation period. The removal of this peak throughout the irradiation is in good agreement with the formation of the diol functionality in **P1** in

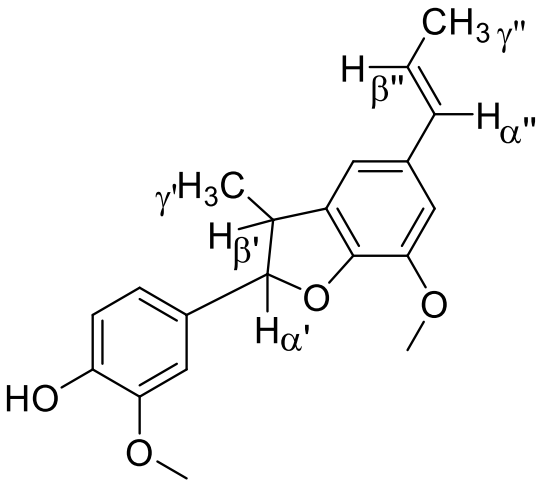

Figure 4. Detailed structure of β-5 substrate showing the position of the proton environments discussed in the NMR experiment.

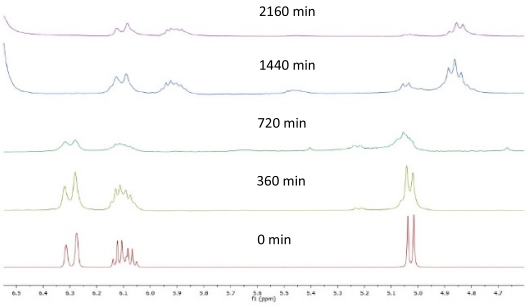

Figure 5. ^{1}H NMR (CD_3CN) spectra stack showing the difference in chemical shift and multiplicity of the doublet at 5.06 ppm throughout a 36 h irradiation period. Reaction solution contained 50 mg of substrate, 50 mg catalyst in a 3 ml reaction solution in the 75:25 proportion with CD_3CN:H_2O. Reaction vessel was a quartz tube of diameter 9 mm and irradiated from the side using same LED as setup shown in figure S2.

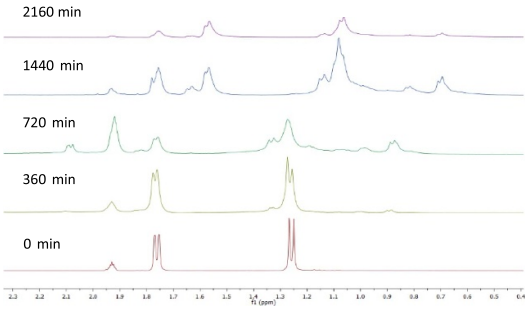

Figure 6. NMR stack showing the difference in chemical shift and multiplicity of the doublet at $\delta = 1.26$ and doublet of doublets at $\delta = 1.76$ throughout a 36 h irradiation period. Reaction solution contained 50 mg of substrate, 50 mg catalyst in a 3 ml reaction solution in the 75:25 proportion with CD_3CN:H_2O. Reaction vessel was a quartz tube of diameter 9 mm and irradiated from the side using same LED as setup shown in figure S2.

figure 3. The formation of a doublet at 1.57 ppm indicates that the methyl group is α to a CH(OH) functionality leading to a shift of the peak upfield.

A key observation made when monitoring the degradation of the β-5 model, was that guaiacol was never detected in the product stream. At this stage of the research it is unknown why this is the case considering that it should be produced following the elimination reaction to form product **P2**. Guaiacol was also used as a substrate for photocatalysis (figure S9) with a clear response noted under both photolytic (UV light only) and photocatalytic conditions. This observation was unexpected considering that there was no photolytic response of the β-5 model in the presence of UV irradiation alone. Therefore, it is proposed that the stability

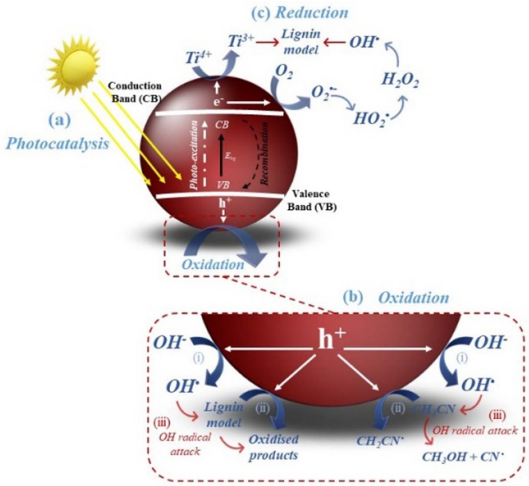

Figure 7. Overview of the potential photocatalytic degradation of lignin models which shows (a) the photocatalysis mechanism; (b) oxidation reactions at the valence band including (1) $OH^{\bullet}$ formation, (2) direct hole oxidation and (3) $OH^{\bullet}$ attack of lignin models and CH_3CN; (c) the formation of $O_2^{\bullet-}$ at the conduction band and $OH^{\bullet}$ generation via H_2O_2 fission.

of the β-5 dimer is determined by either sterics or electronics. The guaiacyl side chain in the β-5 dimer was not cleaved when there was no catalyst present in the reaction solution, therefore electron donation from the benzofuran ring could aid in stabilisation of the guaiacyl ring. Conversely, the electron donating ability of both the phenol and the methoxy on the guaiacyl sidechain in the substrate would in turn confer electronic stability towards the benzofuran ring which lies at the centre of the compound. On the other hand, if it was direct hole oxidation which was occurring at the surface of the catalyst, the structure and conformation of the β-5 dimer, when bound, could be providing steric shielding thus preventing the scission of the bond which connects the guaiacyl sidechain to the rest of the molecule. At this stage in the study, it is plausible to assume that the guaiacyl sidechain, when liberated from the parent molecule, either proceeds to react with other radical species or is broken down via a different mechanism under the reaction conditions.

The complexity of the reactions taking place during the degradation of the β-5 model present a challenge when determining the exact photocatalytic processes which may be responsible. Based on the previous discussion, along with the identification of the reaction intermediates, figure 7 provides an overview of the expected processes occurring, highlighting three key parameters which require consideration; the role of CH_3CN, catalyst-substrate binding and the generation and role of ROS. Previous studies have suggested a range of mechanisms that are dictated by the catalyst and structure of the model compound, however, the exact role the solvent may play is yet to be discussed in detail. In this study, CH_3CN could significantly impact both the rate of degradation and product formation pathway.

In an aerated-aqueous system, model compound or pollutant degradation can result via either direct hole or ROS oxidation generated on the surface of the photocatalyst. The presence of CH_3CN and structure of the model compounds, however, significantly increases the complexity of this process. CH_3CN may create competition for active sites at the TiO_2 surface, which could inhibit $OH^{\bullet}$ formation and substrate binding while also scavenging radicals and valence band holes. Figure 7(b) shows the potential to form $CH_2CN^{\bullet}$ (2) along with CH_3OH and $CN^{\bullet}$ (3). These pathways have previously been reported with evidence suggesting CH_3CN adsorption is favoured over water on the TiO_2 surface [38]. Furthermore, literature has also shown that CH_3CN can undergo a reaction with surface basic sites on TiO_2 P25 and generate acetamide-like species that are 'highly resistant to photodegradation' [38, 39, 45]. In contrast however, the same studies have also shown that on TiO_2 Merck, CH_3CN is adsorbed as is and does not undergo a physical transformation. Therefore, in the system described here, it likely that the TiO_2 P25 surface sites became inactive due to the formation of acetamide-like species. While these processes could inhibit photocatalysis, it is interesting to note that significant model compound degradation was still observed. Oxidation is therefore thought to primarily occur via direct hole oxidation and ROS attack, figures 7(b) and (c). The former is facilitated by the adsorption of β-5 to the TiO_2 surface, while the latter is dictated by both the diffusion capability and type of ROS produced along with the scavenging/inhibiting effect of CH_3CN. The potential radical scavenging effect of CH_3CN was confirmed via the use of coumarin as a probe molecule (see figure S15) [46, 47]. The production of 7-hydroxycoumarin was monitored as an indication of OH radical formation in a system containing 50% CH_3CN and 100% H_2O. While both systems showed the presence of 7-hydroxycoumarin, which confirmed the generation of OH radicals, there was a 2.2-fold increase in fluorescent intensity

(emission $\lambda_{max} = 456$ nm) after 60 min irradiation in the H_2O system. Despite the decrease in $OH^{\bullet}$ production, the data did also confirm the presence of the radical which was a significant observation and suggests that β-5 degradation was still capable of occurring via OH radical attack. Given that surface adsorption was observed, it is feasible to assume direct hole oxidation had taken place, however, this was likely to be enhanced by ROS attack. Furthermore, the diffusion of radicals from the surface may have additionally played a role in the mechanism. This observation could be further supported by literature which has stated CH_3CN as the reaction solvent has the ability to aid in the stabilisation of the $OH^{\bullet}$, which would facilitate both radical diffusion and subsequently β-5 degradation [41]. In addition, it is worth noting that conduction band pathways could play direct and indirect roles in the degradation process, (figure 7(c)). While literature has reported species such as $O_2^{\bullet -}$ and/or Ti^{3+} are capable of weakening C–O bonds [28], $O_2^{\bullet -}$ can also facilitate H_2O_2 formation and subsequently increase $OH^{\bullet}$ production. As discussed in one of our recent publications [42], this process can occur via two mechanisms; H_2O_2 can act as a direct electron acceptor at the conduction band of the catalyst instead of O_2, which has been reported to be the more thermodynamically favourable reaction ($E_0 = 0.72$ for H_2O_2 reduction and $E_0 = -0.13$ for O_2 reduction) (equation (1)) [43, 44]. Alternatively, any H_2O_2 that is not reduced at the conduction band is free to react with the superoxide (equations (2) and (3)). Direct oxidation of H_2O_2 can also occur via reaction with photogenerated holes (and OH radicals), which results in the generation of the superoxide anion radical. In relation to such a system, the presence of CH_3CN may be favourable if the solvent is reacting at the valence band and supressing recombination, which accelerates reactions at the conduction band

$$e_{CB}^{-} + H_2O_2 \rightarrow OH^{\bullet} + OH^{-} \tag{1}$$

$$e_{CB}^{-} + O_2 \rightarrow O_2^{\bullet -} \tag{2}$$

$$O_2^{\bullet -} + H_2O_2 \rightarrow OH^{\bullet} + OH^{-} + O_2. \tag{3}$$

4. Conclusions

The use of semiconductor photocatalysis for the degradation of the key β-5 lignin linkage has been demonstrated. The results of the investigation have shown that, unlike other linkage molecules in lignin, the process is dominated by a photocatalytic process, mediated by TiO_2, rather than a direct photolytic mechanism. The mechanistic pathway has been explored through the use of HPLC, NMR and LC–MS and the results of this study have demonstrated that hydroxyl radical attack on the unsaturated sidechain was a key initial step in the process. This study has shown that the photocatalytic degradation process is however complex, with a number of factors influencing the degradation of the molecule including the ROS, the binding of the substrate to the photocatalyst surface and the role of CH_3CN. Overall TiO_2 photocatalysis appears to be an effective method for the degradation of this important linkage within lignin.

Data availability statement

The data that support the findings of this study are available upon reasonable request from the authors. Supporting data are openly available on Queen's University, Belfast Research Portal, http://pure.qub.ac.uk/portal/en/datasets/search.html.

Acknowledgments

Dr Nathan Skillen would like to acknowledge the RCUK-funded Supergen Bioenergy Hub 2018 project (EP/S000771/1) for funding his research. Mr Christopher Murnaghan would like to acknowledge EPSRC for funding his studentship under project EP/N509541/1. We would like to acknowledge the EPSRC project EP/S018077/1 and Dr Peter Knipe for access to the LC–MS instrument. We are also grateful to Mr Jamie Sweet for assistance with the LC–MS and helpful conversations.

Conflicts of interest

There are no conflicts to declare.

ORCID iDs

Christopher W J Murnaghan https://orcid.org/0000-0001-6550-9703
Peter K J Robertson https://orcid.org/0000-0002-5217-661X

References

[1] Liu X, Duan X, Wei W, Wang S and Ni B-J 2019 Photocatalytic conversion of lignocellulosic biomass to valuable products *Green Chem.* **21** 4266–89
[2] Speltini A, Sturini M, Dondi D, Annovazzi E, Maraschi F, Caratto V, Profumo A and Buttafava A 2014 Sunlight-promoted photocatalytic hydrogen gas evolution from water-suspended cellulose: a systematic study *Photochem. Photobiol. Sci.* **13** 1410–9
[3] Chang C, Skillen N, Nagarajan S, Ralphs K, Irvine J T S, Lawton L and Robertson P K J 2019 Using cellulose polymorphs for enhanced hydrogen production from photocatalytic reforming *Sustain. Energy Fuels* **3** 1971–5
[4] Caravaca A, Jones W, Hardacre C and Bowker M 2016 H_2 production by the photocatalytic reforming of cellulose and raw biomass using Ni, Pd, Pt and Au on titania *Proc. R. Soc.* A **472**
[5] Zhang L, Wang W, Zeng S, Su Y and Hao H 2018 Enhanced H_2 evolution from photocatalytic cellulose conversion based on graphitic carbon layers on TiO_2/NiO_x *Green Chem.* **20** 3008–13
[6] Zhang G, Ni C, Huang X, Welgamage A, Lawton L A, Robertson P K J and Irvine J T S 2016 Simultaneous cellulose conversion and hydrogen production assisted by cellulose decomposition under UV-light photocatalysis *Chem. Commun.* **52** 1673–6
[7] Hao H, Zhang L, Wang W and Zeng S 2018 Facile modification of titania with nickel sulfide and sulfate species for the photoreformation of cellulose into hydrogen *Chem. Sus. Chem.* **11** 2810–7
[8] Wu X, Fan X, Xie S, Lin J, Cheng J, Zhang Q, Chen L and Wang Y 2018 Solar energy-driven lignin-first approach to full utilization of lignocellulosic biomass under mild conditions *Nat. Catal.* **1** 772–80
[9] Wakerley D W, Kuehnel M F, Orchard K L, Ly K H, Rosser T E and Reisner E 2017 Solar-driven reforming of lignocellulose to H_2 with a CdS/CdO_x photocatalyst *Nat. Energy* **2** 17021
[10] Kadam S R, Mate V R, Panmand R P, Nikam L K, Kulkarni M V, Sonawane R S and Kale B B 2014 A green process for efficient lignin (biomass) degradation and hydrogen production via water splitting using nanostructured C, N, S-doped ZnO under solar light *RSC Adv.* **4** 60626–35
[11] Wang L, Zhang Q, Chen B, Bu Y, Chen Y, Ma J, Rosario-Ortiz F L and Zhu R 2020 Some issues limiting photo(cata)lysis application in water pollutant control: a critical review from chemistry perspectives *Water Res.* **174** 115605
[12] Machado A E H, Furuyama A M, Falone S Z, Ruggiero R, Da Silva Perez D and Castellan A 2000 Photocatalytic degradation of lignin and lignin models, using titanium dioxide: the role of the hydroxyl radical *Chemosphere* **40** 115–24
[13] Da Silva Perez D, Castellan A, Grelier S, Terrones M G H, Machado A E H, Ruggiero R and Vilarinho A L 1998 Photochemical bleaching of chemical pulps catalyzed by titanium dioxide *J. Photochem. Photobiol.* A **115** 73–80
[14] Crestini C and D'Auria M 1996 Photodegradation of lignin: the role of singlet oxygen *J. Photochem. Photobiol.* A **101** 69–73
[15] Önnerud H, Zhang L, Gellerstedt G and Henriksson G 2002 Polymerization of monolignols by redox shuttle-mediated enzymatic oxidation: a new model in lignin biosynthesis I *Plant Cell* **14** 1953–62
[16] Zakzeski J, Bruijnincx P C A, Jongerius A L and Weckhuysen B M 2010 The catalytic valorization of ligning for the production of renewable chemicals *Chem. Rev.* **110** 3552–99
[17] Mukhtar A, Zaheer M, Saeed M and Voelter W 2017 Synthesis of lignin model compound containing a β-*O*-4 linkage *Z. Nat. Forsch.* B **72** 119–24
[18] Graham Forsythe W, Garrett M D, Hardacre C, Nieuwenhuyzen M and Sheldrake G N 2013 An efficient and flexible synthesis of model lignin oligomers *Green Chem.* **15** 3031–8
[19] Katahira R, Kamitakahara H, Takano T and Nakatsubo F 2006 Synthesis of β-O-4 type oligomeric lignin model compound by the nucleophilic addition of carbanion to the aldehyde group *J. Wood Sci.* **52** 255–60
[20] Lancefield C S and Westwood N J 2015 The synthesis and analysis of advanced lignin model polymers *Green Chem.* **17** 4980–90
[21] Hanson S K, Baker R T, Gordon J C, Scott B L and Thorn D L 2010 Aerobic oxidation of lignin models using a base metal vanadium catalyst *Inorg. Chem.* **49** 5611–8
[22] Watson P A, Wright L J and Fullerton T J 1993 Reactions of metal ion complexes with lignin model compounds, part II. Fe(TSPc) catalyzed formation of oxidized products in the absence of oxygen *J. Wood Chem. Technol.* **13** 391–409
[23] Lin J Y and Lin K Y A 2019 Catalytic conversion of a lignin model compound to value-added products using Cu/TEMPO-catalyzed aerobic oxidation *Biomass Convers. Biorefin.* **9** 617–23
[24] Rahimi A, Azarpira A, Kim H, Ralph J and Stahl S S 2013 Chemoselective metal-free aerobic alcohol oxidation in lignin *J. Am. Chem. Soc.* **135** 6415–8
[25] Yu Y X, Xu Y, Wang T J, Ma L L, Zhang Q, Zhang X H and Zhang X 2013 *In-situ* hydrogenation of lignin depolymerization model compounds to cyclohexanol *J. Fuel Chem. Technol.* **41** 443–8
[26] Binder J B, Gray M J, White J F, Zhang Z C and Holladay J E 2009 Reactions of lignin model compounds in ionic liquids *Biomass Bioenergy* **33** 1122–30
[27] Cox B J, Jia S, Zhang Z C and Ekerdt J G 2011 Catalytic degradation of lignin model compounds in acidic imidazolium based ionic liquids: hammett acidity and anion effects *Polym. Degrad. Stab.* **96** 426–31
[28] Luo N, Wang M, Li H, Zhang J, Liu H and Wang F 2016 Photocatalytic oxidation-hydrogenolysis of lignin β-O-4 models via a dual light wavelength switching strategy *ACS Catal.* **6** 7716–21
[29] Chen J, Liu W, Song Z, Wang H and Xie Y 2018 Photocatalytic degradation of β-O-4 lignin model compound by In_2S_3 nanoparticles under visible light irradiation *Bioenergy Res.* **11** 166–73
[30] Luo J, Zhang X, Lu J and Zhang J 2017 Fine tuning the redox potentials of carbazolic porous organic frameworks for visible-light photoredox catalytic degradation of lignin β-O-4 models *ACS Catal.* **7** 5062–70
[31] Han G, Yan T, Zhang W, Zhang Y C, Lee D Y, Cao Z and Sun Y 2019 Highly selective photocatalytic valorization of lignin model compounds using ultrathin metal/CdS *ACS Catal.* **9** 11341–9
[32] Zhang J 2018 Conversion of lignin models by photoredox catalysis *Chem. Sus. Chem.* **11** 3071–80
[33] Kärkäs M D, Bosque I, Matsuura B S and Stephenson C R J 2016 Photocatalytic oxidation of lignin model systems by merging visible-light photoredox and palladium catalysis *Org. Lett.* **18** 5166–9

[34] Fang Z and Meier M S 2018 Toward the oxidative deconstruction of lignin: oxidation of β-1 and β-5 linkages *Org. Biomol. Chem.* **16** 2330–41
[35] Daina S, Orlandi M, Bestetti G, Wiik C and Elegir G 2002 Degradation of β-5 lignin model dimers by Ceriporiopsis subvermispora *Enzyme Microb. Technol.* **30** 499–505
[36] Lin J, Wu X, Xie S, Chen L, Zhang Q, Deng W and Wang Y 2019 Visible-light-driven cleavage of C−O linkage for lignin valorization to functionalized aromatics *Chem. Sus. Chem.* **12** 5023–31
[37] Krishna M P S M, Moses G S and Krishna K V S G M 2009 Synthesis and photocatalytic degradation of dimer model compounds of lignin over UV irradiated TiO_2 *Asian J. Chem.* **21** 11–22
[38] Addamo M, Augugliaro V, Coluccia S, Faga M G, García-López E, Loddo V, Marcì G, Martra G and Palmisano L 2005 Photocatalytic oxidation of acetonitrile in gas–solid and liquid–solid regimes *J. Catal.* **235** 209–20
[39] Augugliaro V, Coluccia S, García-López E, Loddo V, Marcì G, Martra G, Palmisano L and Schiavello M 2005 Comparison of different photocatalytic systems for acetonitrile degradation in gas–solid regime *Top. Catal.* **35** 237–44
[40] Leopold B 1950 Aromatic keto- and hydroxy-polyethers as lignin models III *Acta Chem. Scand.* **2** 1523–37
[41] Mitroka S, Zimmeck S, Troya D and Tanko J M 2010 How solvent modulates hydroxyl radical reactivity in hydrogen atom abstractions? *J. Am. Chem. Soc.* **132** 2907–13
[42] Kelly J, McDonnell C, Skillen N, Manesiotis P and Robertson P K J 2021 Enhanced photocatalytic degradation of 2-methyl-4-chlorophenoxyacetic acid (MCPA) by the addition of H_2O_2 *Chemosphere* **275** 130082
[43] Jaeger C D and Bard A J 1979 Spin trapping and electron spin resonance detection of radical intermediates in the photodecomposition of water at TiO_2 particulate systems *J. Phys. Chem.* **83** 3146–52
[44] Cornish B J P A, Lawton L A and Robertson P K J 2000 Hydrogen peroxide enhanced photocatalytic oxidation of microcystin-lR using titanium dioxide *Appl. Catal.* B **25** 59–67
[45] Davit P, Martra G, Coluccia S, Augugliaro V, García López E, Loddo V, Marcì G, Palmisano L and Schiavello M 2003 Adsorption and photocatalytic degradation of acetonitrile: FT-IR investigation *J. Mol. Catal.* A **204–205** 693–701
[46] Buck C, Skillen N, Robertson J and Robertson P K J 2018 Photocatalytic OH radical formation and quantification over TiO_2 P25: producing a robust and optimised screening method *Chin. Chem. Lett.* **29** 773–7
[47] Nagarajan S, Skillen N C, Fina F, Zhang G, Randorn C, Lawton L A, Irvine J T S and Robertson P K J 2017 Comparative assessment of visible light and UV active photocatalysts by hydroxyl radical quantification *J. Photochem. Photobiol.* A **334** 13–9